# Control of Rydberg-state population with realistic femtosecond laser pulses

Janne Solanpää* and Esa Räsänen†
*Laboratory of Physics, Tampere University of Technology, Tampere FI-33101, Finland*

(Received 27 August 2018; published 15 November 2018)

We investigate computationally a method for ultrafast preparation of alkali-metal atoms in their Rydberg states using a three-dimensional model potential in the single active electron approximation. By optimizing laser pulse shapes that can be generated with modern waveform synthesizers, we propose pulses for controlling the population transfer from the ground state to a preselected set of Rydberg states. Dynamical processes under the optimized pulses are shown to be much more complicated than in the traditional optical two-photon preparation of Rydberg states.

DOI: 10.1103/PhysRevA.98.053422

## I. INTRODUCTION

Rydberg states have been observed in numerous systems including, e.g., alkali-metal atoms [1] and larger systems such as water [2] and NO molecules [3]. Their features include long lifetimes [1], macroscopic extent of the electron wave function, and large dipole moments [4]. These features make them prime candidates for applications in, e.g., quantum information and quantum computing [5]. They are also of fundamental interest in the study of quantum chaos [6].

Experimental preparation of isolated alkali-metal atoms in Rydberg states can be achieved with two-photon absorption [4]. In rubidium, the successive absorption of 480- and 780-nm photons can excite the valence electron to a high-$n$ Rydberg state with up to 80 % probability [7]. However, the two-photon absorption technique requires (i) tuning of the laser frequencies to the desired resonances and (ii) long irradiation durations to achieve reasonable yields [7].

Addressing these drawbacks may be achieved by using laser pulses with tailored temporal profiles. Standard techniques exist for the production of tailored femtosecond laser pulses [8], and their applicability has been demonstrated for controlling various dynamical phenomena in atoms such as above-threshold ionization [9,10] and high-order-harmonic generation [11–16,17(a),18]. Population and excitation control of atoms with femtosecond pulses has been studied to some extent both experimentally [17(b),19–21] and computationally [19,20]. However, control of the excitation to high-$n$ Rydberg states using multicolor fields from modern light-field synthesizers has yet to be demonstrated.

In this work, we investigate the applicability of tailored femtosecond laser pulses to ultrafast excitation of alkali atoms to their Rydberg states. Using a computational optimization scheme similar to Ref. [10], we optimize a set of experimentally feasible pulse parameters and find optimal laser pulses that can achieve up to 20% population transfer to the targeted states. The pulse durations are typically less than a few dozen femtoseconds—demonstrating the possibility of ultrafast Rydberg state preparation.

This paper is organized as follows. In Sec. II, we introduce the numerical methods and the optimization scheme. In Sec. III, we discuss the optimal pulse shapes for ultrafast Rydberg state preparation and investigate the underlying dynamical processes. Finally, in Sec. IV we summarize our findings.

## II. NUMERICAL METHODS

As a prototype atom for optimization simulations, we use lithium within the single active electron (SAE) approximation with the static potential $V_0(r)$ introduced in Ref. [22]. The optimization scheme is independent of the precise atomic model, and the scheme is readily applicable to other models of alkali-metal atoms. The laser-electron interaction is included in the dipole approximation, yielding the velocity gauge Hamiltonian (in Hartree atomic units [23])

$$\hat{H}(t) = \frac{\hat{\mathbf{p}}^2}{2} + V_0(\hat{\mathbf{r}}) + A_z(t)\hat{p}_z, \tag{1}$$

where we have restricted ourselves to linearly polarized laser fields, and the diamagnetic $\frac{A(t)^2}{2}$ term has been gauge transformed away.

Our goal is to transfer the maximum amount of population from the initial state, $2s$, (with zero azimuthal quantum number, $m = 0$) to a certain set $\mathcal{I}$ of Rydberg states $|\phi_{n,l}\rangle$ (preserving $m = 0$). This can be achieved by maximizing the target functional

$$G[\mathbf{u}] = \sum_{|\phi_{n,l}\rangle \in \mathcal{I}} |\langle \phi_{n,l} | \psi(T_{\max})\rangle|^2, \tag{2}$$

where $\mathbf{u}$ is the set of optimizable parameters and $|\psi(T_{\max})\rangle$ is the electron state at the end of the laser pulse.

The optimizable parameters $\mathbf{u}$ define the temporal shape of the laser vector potential $A_z[\mathbf{u}](t)$. Similarly to the approaches in Refs. [10,24], the pulse is constructed as a superposition of

*janne@solanpaa.fi
†esa.rasanen@tut.fi

 

multiple *channels*, each with a single central wavelength, i.e.,

$$A_z(t) = \sum_{i=1}^{N} \frac{A_i}{\omega_i} \mathrm{env}(t-\tau_i, \sigma_i) \cos\left[\omega_i(t-\tau_i)+\phi_i\right], \quad (3)$$

where $A_i$, $\omega_i$, $\tau_i$, $\phi_i$, and $\sigma_i$ are the amplitude, frequency, time of envelope maximum, carrier-envelope phase, and envelope full width at half maximum (FWHM) of each channel. The channel envelopes are given by

$$\mathrm{env}(t-\tau,\sigma) = \begin{cases} \exp\left[-\frac{\log(2)}{1-(\frac{t-\tau}{2\sigma})^2}\left(\frac{t-\tau}{\sigma}\right)^2\right], & |t-\tau| < 2\sigma \\ 0, & \text{otherwise} \end{cases}. \quad (4)$$

This is a modified Gaussian which goes to zero at twice the FWHM, and it is infinitely times differentiable everywhere. This pulse parametrization allows us to model realistic pulse shapes that can be generated with modern light field synthesizers [8].

Calculation of the target functional in Eq. (2) for each pulse shape requires us to (i) compute stationary states $|\phi_{n,l}\rangle$ of the system and (ii) propagate the initial state of the system under the laser vector potential. The stationary states are obtained by solving the effective radial equation for each angular quantum number $l$ with first-order finite differences. Time propagation of the electron wave function is carried out with the QPROP software, version 2.0 [25] using the Crank-Nicolson scheme [26]. For simulation parameters, we have used the radial grid spacing 0.1 a.u. (0.005 nm), radial grid length 300 a.u. (16 nm), $l$ quantum numbers up to 50, imaginary absorbing potential of width 50 a.u. (2.6 nm), and time step 0.02 a.u. (0.5 as) for the simulations. Convergence of a few selected results was checked with higher accuracy.

The QPROP software was modified and wrapped for use within PYTHON 3 [27] for interfacing with the optimization library NLOPT [28]. Optimization is performed with a two-step scheme: Global optimization is carried out with *multi-level single-linkage* (MLSL) algorithm [29], which essentially restarts local optimization while avoiding previously found local extrema [28], and for local optimization we use the derivative-free, trust-region-based algorithm called the *constrained optimization by linear approximations* (COBYLA) method [28,30]. This derivative-free optimization scheme does not require the computation of the gradient of Eq. (2).

The optimization routine is provided with one to six different channels with fixed central wavelengths 300 nm, 400 nm, 700.2243 nm, 800 nm, 1.6 $\mu$m, and 2 $\mu$m. The value close to 700 nm is in resonance with the $2s \rightarrow 2p$ transition. Furthermore, each channel is constrained to maximum electric field amplitude of $A_i \leqslant 67$ GV/m. The time of the envelope maximum is allowed to vary $\pm 6$ fs, and the field FWHM of each channel can have values between 2.4 and 15 fs.

## III. OPTIMIZATION RESULTS

A typical optimization process is shown in Fig. 1. It begins with a random initial pulse within the constrained search space, and local optimizer looks for a local maximum of the target functional. After a local maximum has been found, approximately at iteration number 102, the global optimization routine takes over and provides the local optimizer a new initial guess, causing a sharp drop in the target value. A typical optimization simulation runs approximately 100 to 200 optimization steps, providing up to a few local maxima. Optimization of the pulse parameters is indeed crucial for reaching reasonable target populations. In the example of Fig. 1, the optimization starts with a random pulse combination reaching barely 1% target population, but the optimization shapes the pulse to provide up to 5% target population (at iteration number 149).

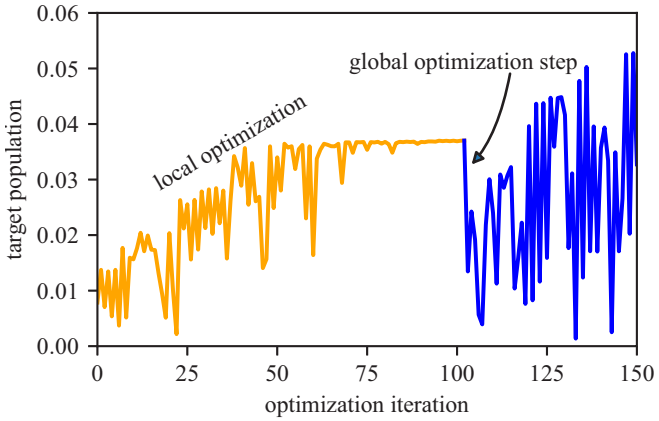


FIG. 1. Total population of the target states as a function of the optimization iterations demonstrating the working principle of the two-step optimization scheme. After convergence of the first local optimization [orange (gray) curve], the global optimizer restarts the local optimizer in a different region of the search space [at iteration number 102, blue (black) curve]. Here we have targeted the states $n = 7, l = 0 \ldots 2$.

The best results for each set of target states are collected in Table I. We only show the best one or two channel combinations for each target, but all possible channel combinations were tested. The optimized target populations range from 90% for the simplest target down to 3% for more difficult to reach target states such as $n = 7$, $l = 4 \ldots 6$. We have also investigated the excitation of the system to a single target state: For $7f$, we have reached up to 2.5% population and for $8i$ up to 1.7%. These moderate populations of single-target states suggest the scheme lacks the finesse to target single Rydberg states. However, due to finding only a few local extrema per target for each channel combination, it may

TABLE I. Summary of maximum achieved target populations for different pulse channel combinations.

| Target | Channels ($\mu$m) | Max. population |
|---|---|---|
| $2p$ | 0.7 | 91% |
| $n = 7, l = 0 \ldots 2$ | 0.8, 0.7, 0.4, 0.3 | 14% |
| | 0.8, 0.7, 0.4 | 5% |
| $n = 7, l = 4 \ldots 6$ | 2, 0.8, 0.7, 0.4 | 6% |
| | 2, 0.8, 0.4 | 3% |
| $n = 7 \ldots 10, l = 4$ | 2, 0.7 | 6% |
| $n = 7 \ldots 10$ | 2, 0.8, 0.7, 0.3 | 23% |
| | 2, 1.6, 0.8, 0.7, 0.3 | 21% |

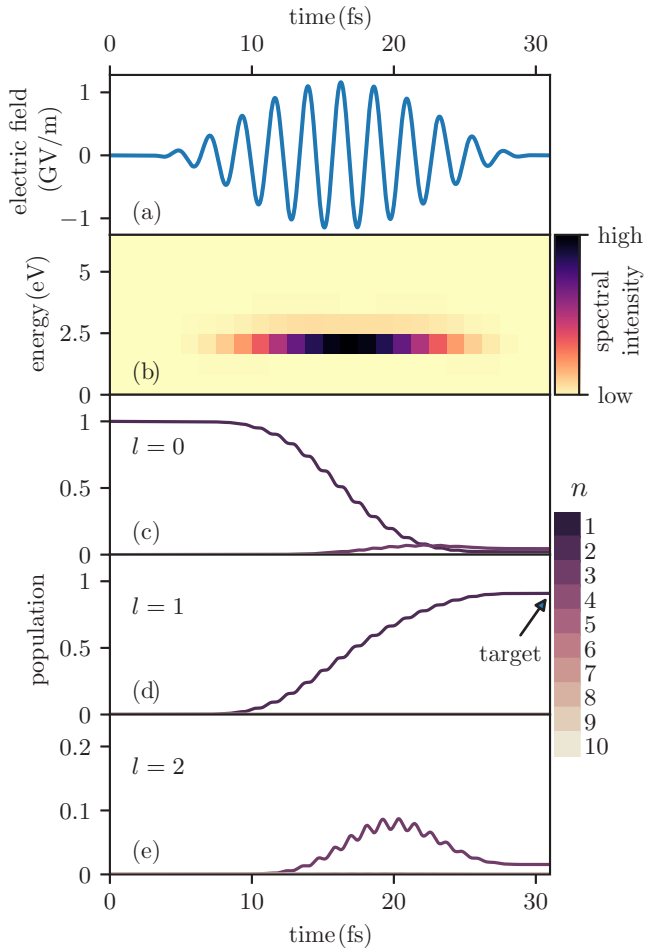


FIG. 2. (a) The optimized laser pulse for populating the $2p$ state, (b) the power spectral density of the laser electric field, and (c)–(e) the populations of the stationary states.

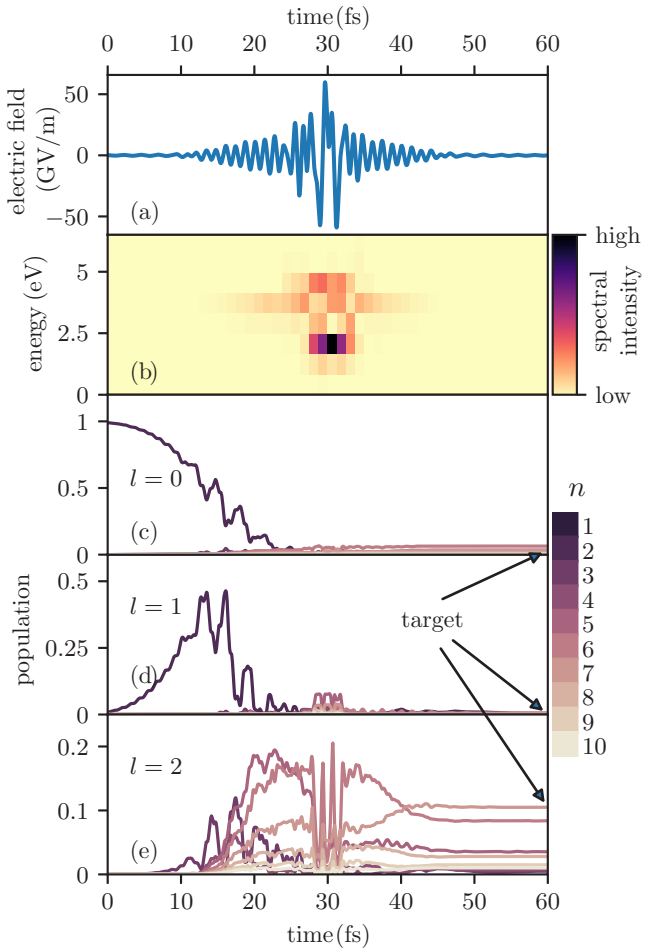


FIG. 3. (a) The optimized laser pulse for populating the set of states $n = 7$, $l = 0 \ldots 2$ using the channels 800, 700, 400, and 300 nm, (b) the power spectral density of the electric field, and (c)–(e) the populations of the stationary states.

be possible to improve these results with more optimization simulations and/or gradient-based algorithms.

The maximum populations in Table I are less than those achieved in previous works on optimal control of population transfer in atoms and molecules, e.g., in Refs. [31,32]. However, one must take into account the extremely constrained pulse combinations required by modern waveform synthesizers. In particular, the pulses with fixed channel wavelengths lack the ability to play with the resonances of the system. Moreover, the Gaussian envelope of each channel forbids any sudden changes in the temporal profiles of the pulses, and shortness of the resulting pulses forces the control scheme to consider multiple complex transitions between the states.

Next we will inspect the population transfer mechanisms behind the optimal pulses for a few select examples from Table I. The simplest transition to consider is $2s \rightarrow 2p$. This is forbidden for hydrogen, but for Li the transition is allowed. This transition also serves as the first step in the optical preparation of Rydberg states through a two-step excitation [4]. We find the optimal population transfer to be achieved with a pulse consisting only of the 700-nm channel—not surprising since the channel is in resonance with the transition. The pulse and the populations of the few lowest states are show in Fig. 2.

The optimal pulse has a small peak electric field to avoid ionization, and a 90% population transfer is achieved with a pulse duration (intensity FWHM) less than 10 fs. Merely increasing the pulse duration would not improve the result since the initial state, $2s$, is already depleted with the current pulse shape. At first, the population transfer $2s \rightarrow 2p$ seems like a simple few-level process. Indeed, a two-level model with the states $2s$ and $2p$ under the laser pulse of Fig. 2 already yields an 80% population transfer. However, even a bound-state model with all states up to $n = 10$ fails to reach the 90% yield of the full model. This suggests either the involvement of very high Rydberg states or perhaps even the continuum in the full population transfer.

Let us turn our attention to ultrafast population of Rydberg states. Targeting the states $n = 7$, $l = 0 \ldots 2$, our scheme yields a solid 14% final population using the channels 800, 700, 400, and 300 nm (see Fig. 3). These channels are mixed with peak electric field ratios of $35 : 1 : 13 : 16$. While the 700-nm channel is relatively weak compared to others, it is of utmost importance and without it the final target population would drop to 0.2%. The optimized population transfer is somewhat akin to the traditional two-step excitation: First the

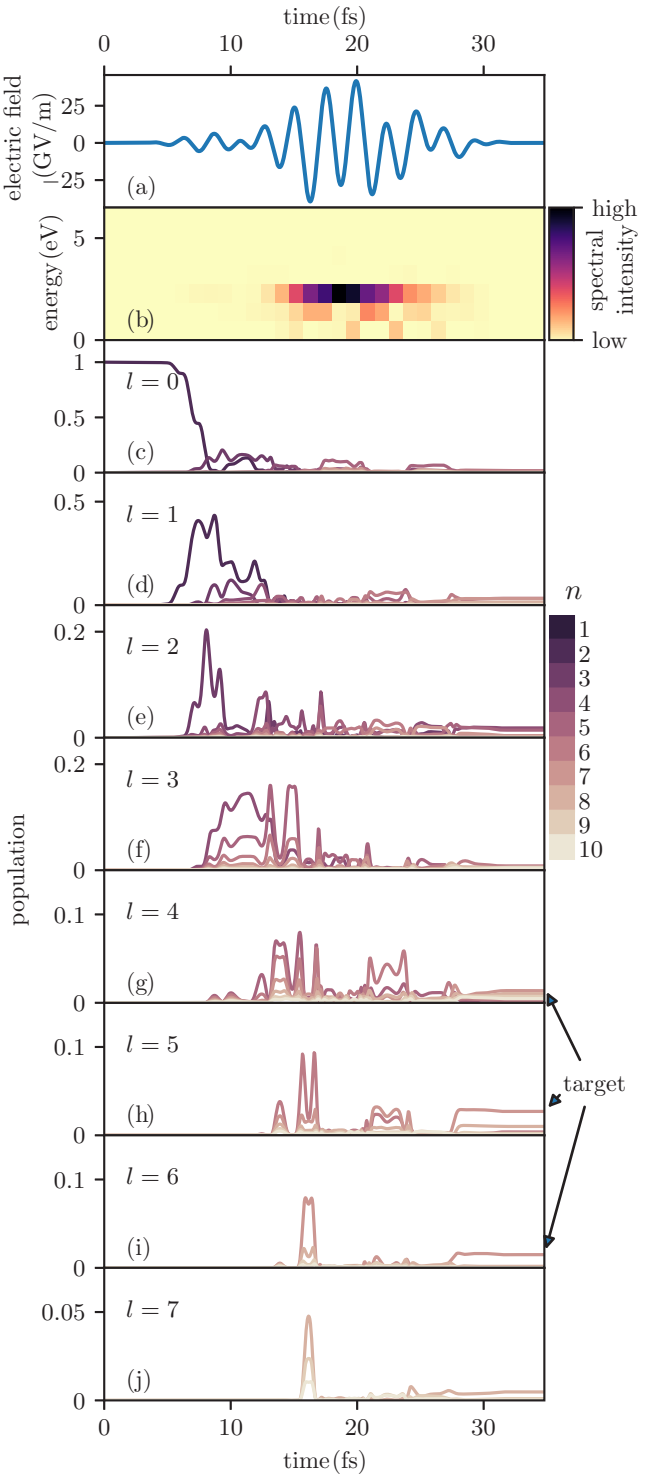


FIG. 4. (a) The optimized laser pulse for populating the set of states $n = 7$, $l = 4 \ldots 6$ using the channels 2 $\mu$m, 800 nm, 700 nm, and 400 nm, (b) the power spectral density of the electric field, and (c)–(j) the populations of the stationary states.

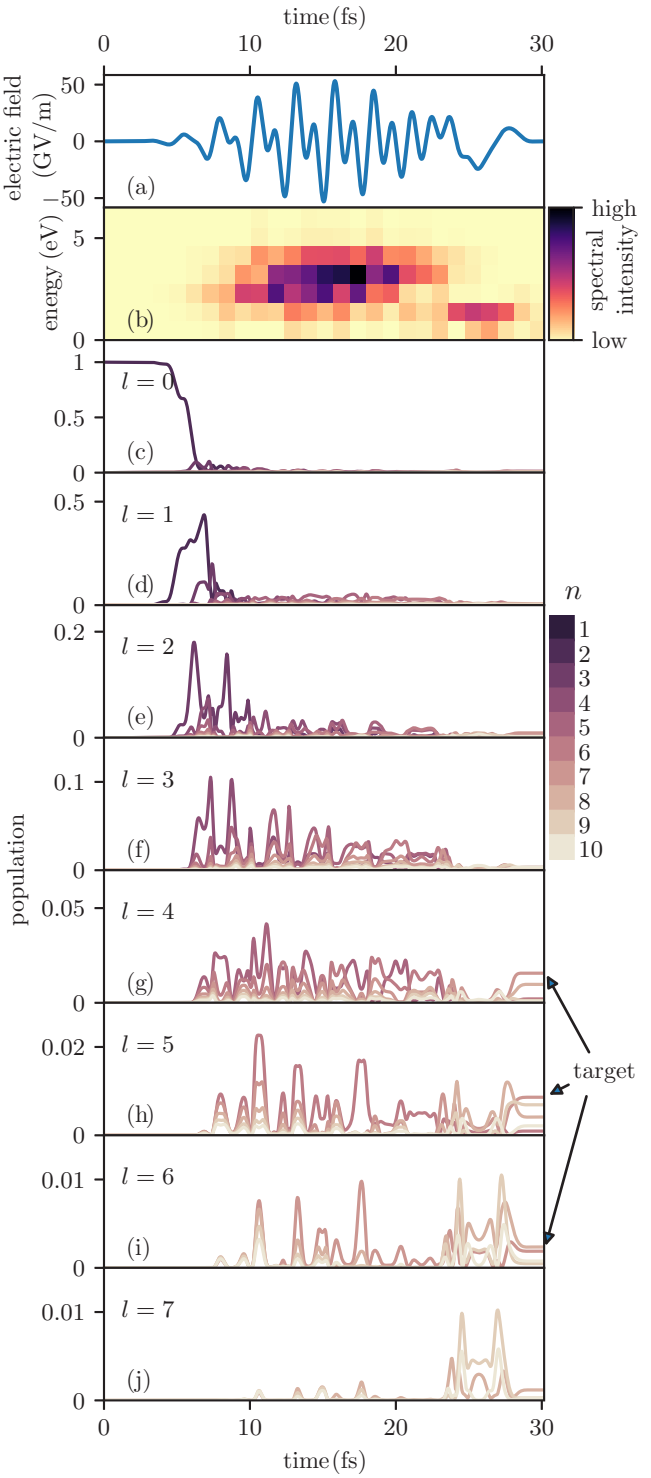


FIG. 5. Same as Fig. 4, but without the 700-nm channel.

electron is excited from $2s$ to $2p$ by the weak 700-nm component; however, the second step is a much more complicated process involving multiple transitions resulting in most of the final target population in the $7d$ state.

Next, we will focus our attention on a more complicated target, $n = 7$, $l = 4 \ldots 6$, which cannot be reached with two-photon absorption, in contrast with the previous example. An optimized pulse of duration less than 30 fs can transfer up to 6% of the electron population to the target states. The pulse, shown in Fig. 4(a), mixes the channels 2 $\mu$m, 800 nm, 700 nm, and 400 nm in ratios of electric field peak amplitude as 1 : 1.8 : 2.25 : 0.04. The 800- and 700-nm channels activate

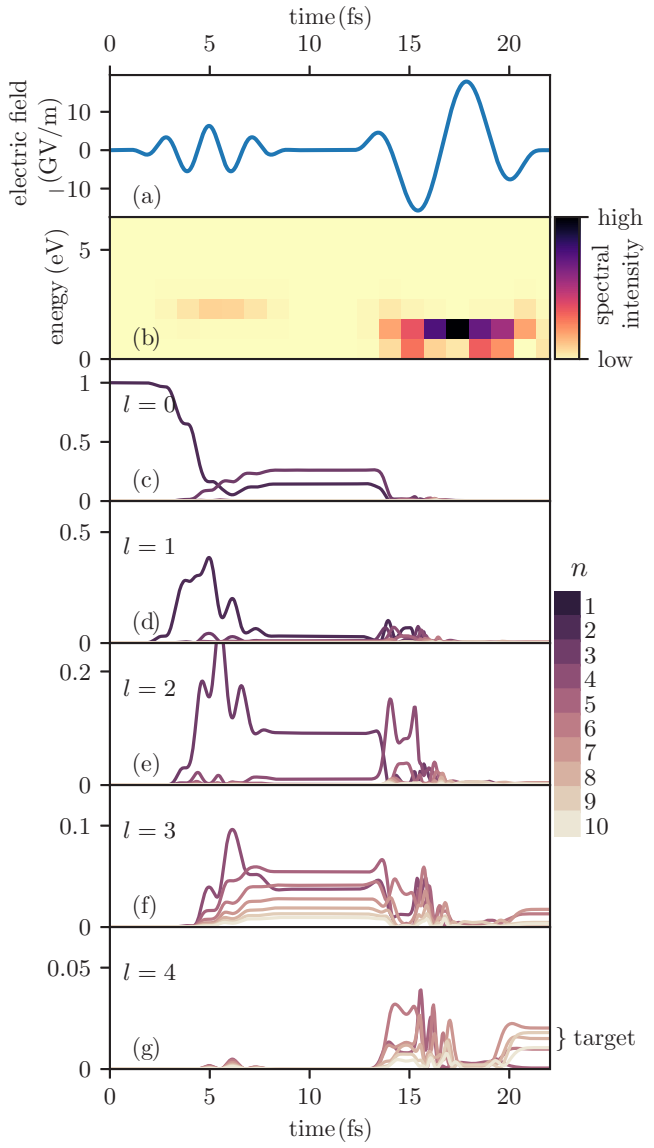


FIG. 6. (a) The optimized laser pulse for populating the set of $l = 4$ states with principal quantum numbers $n = 7 \ldots 10$ consists of first a few-cycle 700-nm primer followed by single-cycle 2-$\mu$m pulse, (b) the power spectral density of the electric field, and (c)–(g) the populations of the stationary states.

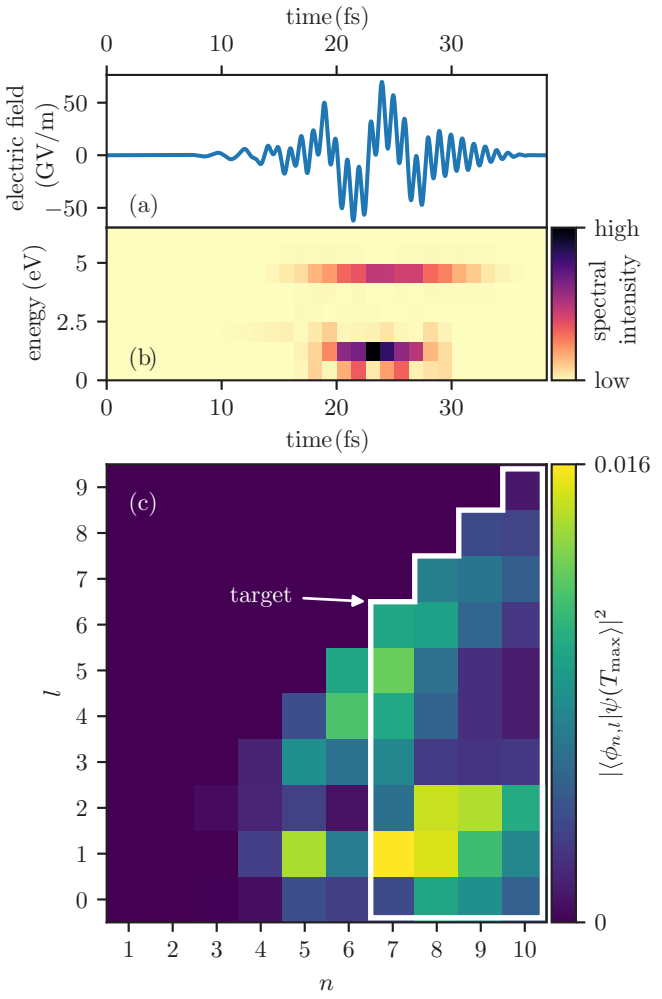


FIG. 7. (a) The optimized laser pulse for populating the set of states $n = 7 \ldots 10$ using the channels 2 $\mu$m, 800 nm, 700 nm, and 300 nm, (b) the power spectral density of the electric field, and (c) the final populations of the stationary states.

simultaneously, while the 2-$\mu$m channel activates 6 fs later than the previous ones. The channels overlap significantly in time, yielding a complicated process for the population transfer. The first few femtoseconds, up to approximately $t = 12$ fs, transfer the population from $2s$ to higher states with $l \approx 1 \ldots 3$, whereas the rest of the pulse makes the electron population oscillate between multiple states and partly ionize.

A question arises of whether the 700-nm pulse is an essential primer to achieve the initial $2s \rightarrow 2p$ excitation. This is not the case, as demonstrated in Fig. 5 where we optimize the same target as previously but *without* the 700-nm channel. A good initial population transfer to the $2p$ state can still be found; however, rest of the population transfer process is naturally different due to different pulse temporal shape.

We will now turn our attention to targeting the population of a single angular quantum number, e.g., $l = 4$ with $n = 7 \ldots 10$. The optimal pulse, shown in Fig. 6(a), is a sequence of 700-nm and 2-$\mu$m channels providing us final target population of 6%. To analyze the population transfer process via pairwise transfer rates, notice first that the state populations $|c_{n,l}|^2 = |\langle\phi_{n,l}|\psi(t)\rangle|^2$ are equivalent in the Schrödinger and interaction pictures of quantum mechanics. In the interaction picture, the expansion coefficients obey the system of ordinary differential equations [33]

$$\frac{d}{dt}c^I_{(n,l)}(t) = -iA_z(t)\sum_{(n',l')} W_{(n,l),(n',l')} \times \exp\{i[E_{(n',l')} - E_{(n,l)}]t\}c^I_{(n',l')}(t), \quad (5)$$

where $W_{(n,l),(n',l')}$ is the $z$ component of the $(n,l),(n',l')$ momentum matrix element in the Schrödinger picture. Now, the pairwise transfer rates are given by

$$T_{(n,l),(n',l')}(t) = A_z(t)^2|W_{(n,l),(n',l')}|\langle\phi^S_{n,l}|\psi^S(t)\rangle|^2. \quad (6)$$

The transfer rates $T$ for the optimized population transfer to $l = 4$, $n = 7 \ldots 10$ are shown as a function of time in the animation that can be found in Supplementary Material [34]. The first, 700-nm pulse excites the system from the initial $2s$ state to a set of $l = 3$ states ($n = 4 \ldots 10$) via $2p$. Some population is left in the $2p$ and $3d$ states. The second, 2-$\mu$m pulse first transfers population leftovers from the $2p$ state via $4d$ state to the $f$ states, and after its first optical cycle, the second pulse transfers the population from the $f$ states to the targeted $g$ states. Because of weak pulses, the system is essentially not ionized, but the rest of the population escapes to higher bound states. Transfer rates seem the obvious choice for interpreting the optimal population transfer processes for each target, but they turn out to be significantly more complicated for most of the other targets.

As a final demonstration, we target the states with principal quantum numbers $n = 7 \ldots 10$ without restrictions to the angular quantum number. Because of the larger number of targeted states, the total target population reaches over 20% with the optimal pulses with the highest yield achieved with the channels 2 $\mu$m, 800 nm, 700 nm, and 400 nm, shown in Fig. 7. Most of the final target population is in low-$l$ states, peaking at $7p$ and $8p$ followed by their neighbours by coupling, $8d$ and $9d$.

## IV. SUMMARY

We have demonstrated the applicability of a few-color femtosecond pulses realizable by modern waveform synthesis [8] to optimal control of population transfer from ground state to a set of Rydberg states. Our control scheme was found to achieve up to 23% Rydberg-state populations when transferring population to a few selected states, but when targeting a single state these experimentally restricted pulse combinations do not seem to allow sufficient control over the excitation process.

Typical simulations with such realistic multicolor waveforms yield complicated dynamical processes which usually cannot be easily interpreted with clear few-step excitation paths. In this respect, our results also demonstrate a very different optimized dynamical process compared to having longer and less constrained pulses, which allows the exploitation of the resonances.

We expect that with refinements to the available pulse configurations and more powerful, gradient-based optimization algorithms one can further increase the total achieved target population. These enhancements could also allow us to target smaller sets of states while still retaining compatibility with experimentally feasible wave forms. In addition, further investigation would be warranted to study the applicability of our scheme to, e.g., the preparation of circular Rydberg states, including field polarization as an additional control knob, and to full multielectron models with possibly even more complicated optimization landscapes.

## ACKNOWLEDGMENTS

The authors are grateful to Prof. Hossein Sadeghpour for insightful discussions and Mika Sarvilahti for the idea regarding the modified Gaussian function. This work was supported by the Academy of Finland (Grants No. 267686 and No. 304458). We also acknowledge CSC—the Finnish IT Center for Science—for computational resources.

[1] See, e.g., C. E. Theodosiou, Phys. Rev. A **30**, 2881 (1984).
[2] H. T. Wang, W. S. Felps, and S. P. McGlynn, J. Chem. Phys. **67**, 2614 (1977).
[3] A. Lagerqvist and E. Miescher, Can. J. Phys. **44**, 1525 (1966).
[4] T. F. Gallagher, *Rydberg Atoms* (Cambridge University Press, Cambridge, UK, 1994).
[5] M. Saffman, T. G. Walker, and K. Mølmer, Rev. Mod. Phys. **82**, 2313 (2010).
[6] P. J. J. Luukko and J.-M. Rost, Phys. Rev. Lett. **119**, 203001 (2017).
[7] T. A. Johnson, E. Urban, T. Henage, L. Isenhower, D. D. Yavuz, T. G. Walker, and M. Saffman, Phys. Rev. Lett. **100**, 113003 (2008).
[8] See, e.g., M. T. Hassan, A. Wirth, I. Grguraš, A. Moulet, T. T. Luu, J. Gagnon, V. Pervak, and E. Goulielmakis, Rev. Sci. Instrum. **83**, 111301 (2012), and references therein.
[9] R. E. Goetz, A. Karamatskou, R. Santra, and C. P. Koch, Phys. Rev. A **93**, 013413 (2016).
[10] J. Solanpää, M. F. Ciappina, and E. Räsänen, J. Mod. Opt. **64**, 1784 (2017).
[11] J. Solanpää, J. A. Budagosky, N. I. Shvetsov-Shilovski, A. Castro, A. Rubio, and E. Räsänen, Phys. Rev. A **90**, 053402 (2014).
[12] A. Castro, A. Rubio, and E. K. U. Gross, Eur. Phys. J. B **88**, 191 (2015).
[13] C. Jin and C. D. Lin, Chin. Phys. B **25**, 094213 (2016).
[14] G.-L. Wang, L.-H. Zhou, S.-F. Zhao, and X.-X. Zhou, Commun. Theor. Phys. **65**, 601 (2016).
[15] D. Peng, M. V. Frolov, L.-W. Pi, and A. F. Starace, Phys. Rev. A **97**, 053414 (2018).
[16] C. Winterfeldt, C. Spielmann, and G. Gerber, Rev. Mod. Phys. **80**, 117 (2008).
[17] (a) Y. Chou, P.-C. Li, T.-S. Ho, and S.-I. Chu, Phys. Rev. A **91**, 063408 (2015); (b) See, e.g., T. Hornung, R. Meier, D. Zeidler, K.-L. Kompa, D. Proch, and M. Motzkus, Appl. Phys. B **71**, 277 (2000), and references therein.
[18] S. Haessler *et al.*, Phys Rev. X **4**, 021028 (2014).
[19] R. Netz, T. Feurer, G. Roberts, and R. Sauerbrey, Phys. Rev. A **65**, 043406 (2002).
[20] B. Chatel, J. Degert, S. Stock, and B. Girard, Phys. Rev. A **68**, 041402 (2003).
[21] A. Präkelt, M. Wollenhaupt, C. Sarpe-Tudoran, and T. Baumert, Phys. Rev. A **70**, 063407 (2004).
[22] W. Schweizer, P. Faßbinder, and R. González-Férez, At. Data Nucl. Data Tables **72**, 33 (1999).
[23] D. R. Hartree, Math. Proc. Camb. Philos. Soc. **24**, 89 (1928).
[24] B. Bódi, E. Balogh, V. Tosa, E. Goulielmakis, K. Varjú, and P. Dombi, Opt. Express **24**, 21957 (2016).

[25] D. Bauer and P. Koval, Comput. Phys. Commun. **174**, 396 (2006).
[26] J. Crank and P. Nicolson, Math. Proc. Cambridge Philos. Soc. **43**, 50 (1947).
[27] Python Software Foundation, PYTHON language reference, version 3.6, https://www.python.org.
[28] S. G. Johnson, The NLOPT nonlinear-optimization package, https://nlopt.readthedocs.io.
[29] A. H. G. R. Kan and G. T. Timmer, Math. Prog. **39**, 27 (1987).
[30] M. J. D. Powell, A Direct Search Optimization Method That Models the Objective and Constraint Functions by Linear Interpolation, in *Advances in Optimization and Numerical Analysis*, edited by S. Gomez and J.-P. Hennart (Kluwer Academic, Dordrecht, 1994), pp. 51–67.
[31] W. Zhu, J. Botina, and H. Rabitz, J. Chem. Phys. **108**, 1953 (1998).
[32] M. Sugawara, Chem. Phys. Lett. **358**, 290 (2002).
[33] See, e.g., J. J. Sakurai and J. Napolitano, *Modern Quantum Mechanics*, 2nd ed. (Cambridge University Press, Cambridge, UK, 2017), or any other standard book on elementary quantum mechanics.
[34] See Supplemental Material at http://link.aps.org/supplemental/10.1103/PhysRevA.98.053422 for these videos visualize the transition rates, excited state populations, and the laser electric field of the electron dynamics in Figs. 3-7.